frontiers in Physics

REVIEW
published: 21 January 2022
doi: 10.3389/fphy.2021.810394

Phase Diagram of Nickelate Superconductors Calculated by Dynamical Vertex Approximation

Karsten Held[1], Liang Si[1,2]*, Paul Worm[1], Oleg Janson[3], Ryotaro Arita[4,5], Zhicheng Zhong[6], Jan M. Tomczak[1] and Motoharu Kitatani[1,4]**

[1]*Institute for Solid State Physics, Vienna University of Technology, Vienna, Austria,* [2]*School of Physics, Northwest University, Xi'an, China,* [3]*Institute for Theoretical Solid State Physics, Leibniz IFW Dresden, Dresden, Germany,* [4]*RIKEN Center for Emergent Matter Sciences (CEMS), Wako, Japan,* [5]*Department of Applied Physics, the University of Tokyo, Bunkyo, Japan,* [6]*Key Laboratory of Magnetic Materials and Devices and Zhejiang Province Key Laboratory of Magnetic Materials and Application Technology, Ningbo Institute of Materials Technology and Engineering (NIMTE), Chinese Academy of Sciences, Ningbo, China*

We review the electronic structure of nickelate superconductors with and without effects of electronic correlations. As a minimal model, we identify the one-band Hubbard model for the Ni $3d_{x^2-y^2}$ orbital plus a pocket around the A-momentum. The latter, however, merely acts as a decoupled electron reservoir. This reservoir makes a careful translation from nominal Sr-doping to the doping of the one-band Hubbard model mandatory. Our dynamical mean-field theory calculations, in part already supported by the experiment, indicate that the Γ pocket, Nd 4*f* orbitals, oxygen 2*p*, and the other Ni 3*d* orbitals are not relevant in the superconducting doping regime. The physics is completely different if topotactic hydrogen is present or the oxygen reduction is incomplete. Then, a two-band physics hosted by the Ni $3d_{x^2-y^2}$ and $3d_{3z^2-r^2}$ orbitals emerges. Based on our minimal modeling, we calculated the superconducting T_c vs. Sr-doping x phase diagram prior to the experiment using the dynamical vertex approximation. For such a notoriously difficult to determine quantity as T_c, the agreement with the experiment is astonishingly good. The prediction that T_c is enhanced with pressure or compressive strain has been confirmed experimentally as well. This supports that the one-band Hubbard model plus an electron reservoir is the appropriate minimal model.

Keywords: electronic structure calculations, dynamical mean field theory, electronic correlation, high-temperature superconductivity, solid state theory

OPEN ACCESS

Edited by:
Matthias Hepting,
Max Planck Institute for Solid State Research, Germany

Reviewed by:
Fabio Bernardini,
University of Cagliari, Italy
Liviu Chioncel,
University of Augsburg, Germany

****Correspondence:***
Karsten Held
held@ifp.tuwien.ac.at
Liang Si
liang.si@ifp.tuwien.ac.at
Motoharu Kitatani
motoharu.kitatani@riken.jp

Specialty section:
This article was submitted to Condensed Matter Physics, a section of the journal Frontiers in Physics

Received: *06 November 2021*
Accepted: *10 December 2021*
Published: *21 January 2022*

Citation:
Held K, Si L, Worm P, Janson O, Arita R, Zhong Z, Tomczak JM and Kitatani M (2022) Phase Diagram of Nickelate Superconductors Calculated by Dynamical Vertex Approximation. Front. Phys. 9:810394. doi: 10.3389/fphy.2021.810394

1 INTRODUCTION

Twenty years ago, Anisimov, Bukhvalov, and Rice [1] suggested high-temperature (T_c) superconductivity in nickelates based on material calculations that showed apparent similarities to cuprates. Subsequent calculations [2–4] demonstrated the potential to further engineer the nickelate Fermi surface by heterostructuring. Two years ago, Li, Hwang et al. [5] discovered superconductivity in Sr-doped $NdNiO_2$ films grown on a $SrTiO_3$ substrate and protected by a $SrTiO_3$ capping layer. These novel $Sr_xNd_{1-x}NiO_2$ films are isostructural and formally isoelectric to the arguably simplest, but certainly not the best superconducting cuprate: infinite layer $CaCuO_2$ [6–9].

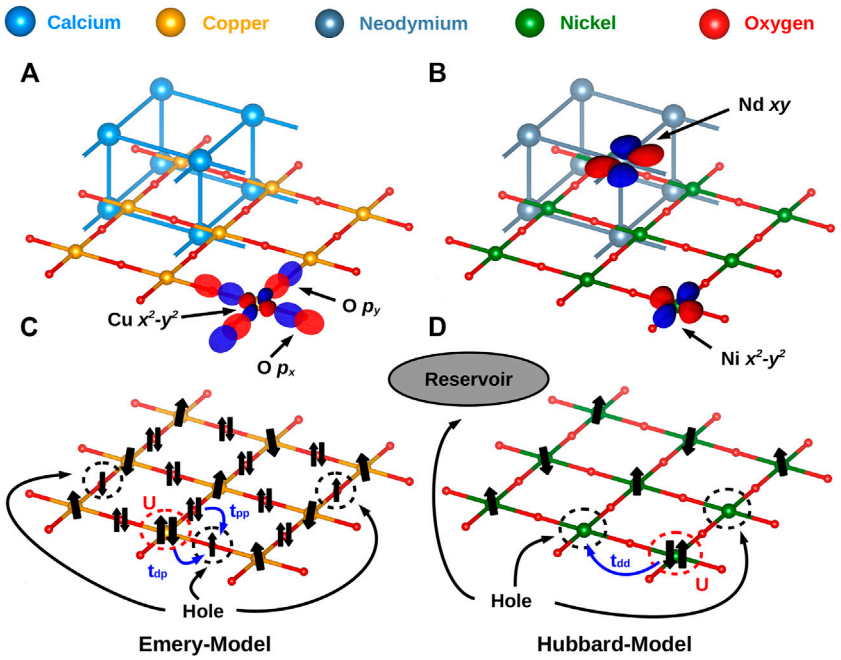

FIGURE 1 | Crystal lattice and most important orbitals for **(A)** cuprates and **(B)** nickelates. **(C)** For cuprates, the arguably simplest model is the Emery model with a half-filled copper $3d_{x^2-y^2}$ band and holes in the oxygen $2p$ orbitals that can hop to other oxygen (t_{pp}) and copper sites (t_{dp}) where double occupations are suppressed by the interaction U. **(D)** For nickelates, we have a Ni-$3d_{x^2-y^2}$-band Hubbard model which, however, only accommodates part of the holes induced by Sr-doping. The others go to the A pocket stemming from the Nd $5d_{xy}$ band and acting as a decoupled reservoir.

However, the devil is in the details, and here cuprates and nickelates differ. For revealing such material-specific differences, band-structure calculations based on density functional theory (DFT) are the method of choice. They serve as a starting point for understanding the electronic structure and, subsequently, the phase diagram of nickelate superconductors. Following the experimental discovery of nickelate superconductivity, and even before that, numerous DFT studies have been published [10–20]. Based on these DFT calculations, various models for the low-energy electronic structure for nickelates and the observed superconductivity have been proposed. Besides the cuprate-like Ni $3d_{x^2-y^2}$ band, DFT shows an A and a Γ pocket which originate from Nd $5d_{xy}$ and $5d_{3z^2-r^2}$ bands, but with major Ni $3d$ admixture in the region of the pocket. The importance of the Ni $3d_{3z^2-r^2}$ orbital has been suggested in some studies [21–24], and that of the Nd-$4f$ orbitals in others [20, 25]. Furthermore, there is the question regarding the relevance of the oxygen $2p$ orbitals. For cuprates, these are, besides the Cu $3d_{x^2-y^2}$ orbitals, the most relevant. Indeed, cuprates are generally believed to be charge-transfer insulators [26]. This leads to the three-orbital Emery model [27] visualized in **Figures 1A,C** as the minimal model for cuprates. The much more frequently investigated Hubbard model [28–30] may, in the case of cuprates, only be considered as an effective Hamiltonian mimicking the physics of the Zhang–Rice singlet [31].

At first glance, nickelates appear to be much more complicated with more relevant orbitals than in the case of the cuprates. In this article, we review the electronic structure of nickelates in comparison to that of cuprates and the arguments for a simpler description of nickelate superconductors, namely, a Hubbard model for the Ni $3d_{x^2-y^2}$ band plus a largely decoupled reservoir corresponding to the A pocket. This A pocket is part of the Nd $5d_{xy}$ band which has, however, a major admixture of Ni $3d_{xz/yz}$ and O $2p_z$ states around the momentum A. This leaves us with **Figures 1B,D** as the arguably simplest model for nickelates [32, 33]. This (our) perspective is still controversially discussed in the literature. However, as we will point out below, a number of experimental observations already support this perspective against some of the early suggestions that other orbitals are relevant. Certainly, other perspectives will be taken in other articles of this series on "Advances in Superconducting Infinite-Layer and Related Nickelates." The simple picture of a one-band Hubbard model, whose doping needs to be carefully calculated since part of the holes in Sr-doped $Sr_xNd_{1-x}NdO_2$ go to the A pocket, allowed us [33] to calculate T_c, see **Figure 5**, at a time when only the T_c for a single doping $x = 20\%$ was experimentally available. To this end, state-of-the-art dynamical vertex approximation (DΓA) [36–38], a Feynman diagrammatic extension of dynamical mean-field theory (DMFT) [39–42] has been used. For such a notoriously difficult to calculate physical quantity as T_c, the agreement of the single-orbital Hubbard model calculation with subsequent experiments [34, 35] is astonishingly good. This further supports the modeling by a single-orbital Hubbard model which, thus,

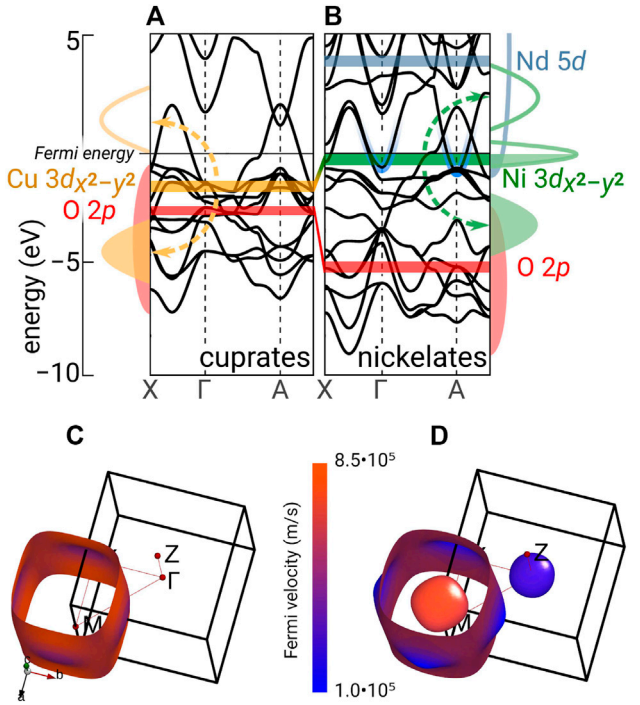

FIGURE 2 | Electronic structures of $CaCuO_2$ **(A)** and $NdNiO_2$ **(B)** exemplifying superconducting cuprates and nickelates. Top: The bars indicate the center of energy for the most important DFT bands. The dashed arrows indicate the correlation-induced splitting of the Cu or Ni $3d_{x^2-y^2}$ band into Hubbard bands, leading to the (schematic) spectral function at the side. Cuprates are charge-transfer insulators with a gap between the O $2p$ and the upper Cu $3d_{x^2-y^2}$ Hubbard band as the lower Cu $3d_{x^2-y^2}$ Hubbard band is below the O $2p$ band. For nickelates, bands with a large La (Nd) $5d$ contribution cross the Fermi energy at Γ and A, self-doping the Ni $3d_{x^2-y^2}$ band away from half-filling. **(C,D)**: Corresponding DFT Fermi surface. For cuprates, DFT shows a single Cu $3d_{x^2-y^2}$ hole–like Fermi surface; for nickelates, there is a similar, slightly more warped Ni $3d_{x^2-y^2}$ Fermi surface and additional small pockets around the Γ and A momentum.

should serve at the very least as a good approximation or a starting point.

The outline of this article is as follows: In **Section 2**,we first compare the electronic structure of nickelates to that of cuprates, starting from DFT but also discussing effects of electronic correlations as described, for example, by DMFT. Subsequently, we argue in **Section 3**, orbital-by-orbital, that the other orbitals besides the Ni $3d_{x^2-y^2}$ and the A pocket are, from our perspective, not relevant. This leaves us with the one-$3d_{x^2-y^2}$-band Hubbard model plus an electron reservoir representing the A pocket of **Figures 1B,D**, which is discussed in **Section 4**, including the translation of Sr-doping to the filling in the Hubbard model and the reservoir. In **Section 5**, we discuss the effect of non-local correlations as described in DΓA and the calculated superconducting phase diagram. **Section 6** shows that topotactic hydrogen, which is difficult to detect in the experiment, completely overhauls the electronic structure and the prevalence of superconductivity. Finally, **Section 7** summarizes the article.

2 ELECTRONIC STRUCTURE: NICKELATES VS. CUPRATES

Let us start by looking into the electronic structure in more detail and start with the DFT results. On a technical note, the calculations presented have been performed using the WIEN2K [43, 44], VASP [45], and FPLO [46] program packages, with the PBE [47] version of the generalized gradient approximation (GGA). For further details, see the original work [33]. **Figure 2** compares the bandstructure of the two simple materials: $CaCuO_2$ and $NdNiO_2$. Here, we restrict ourselves to only the Brillouin zone path along the most relevant momenta for these compounds: Γ (0, 0, 0), X (π, 0, 0), and A (π, π, π). In DFT, both the cuprate and nickelate parent compounds are metals with a prominent Cu or Ni $3d_{x^2-y^2}$ band crossing the Fermi energy. In other aspects, both materials differ (for a review cf [48]): In the case of cuprates, the oxygen bands are much closer to the Fermi energy. Hence, if electronic correlations split the DFT bands into two Hubbard bands as indicated in **Figure 2** by the arrows and the spectral function in the left side panel, we get a charge-transfer insulator [26]. For this charge-transfer insulator, the oxygen $2p$ orbitals are the first orbitals below the Fermi level (E_F) and receive the holes that are induced by doping. The Cu $3d_{x^2-y^2}$ lower Hubbard band is below these oxygen orbitals, and the Cu $3d_{x^2-y^2}$ upper Hubbard band is above the Fermi level. Let us note that we here refer to oxygen $2p$ orbitals and Cu $3d_{x^2-y^2}$ orbitals even though the hybridization between both is very strong. Indeed, the two sets of orbitals strongly mix in the resulting effective DFT bands of **Figure 2**.

Because cuprates are charge-transfer insulators, the one-band Hubbard model can only be considered an effective Hamiltonian mimicking the Zhang–Rice singlet [31]. As already pointed out in the *Introduction*, more appropriate is the Emery model of **Figure 1**. The correlation-induced splitting into the Hubbard bands [40], as well as the Zhang–Rice singlet [49], can be described already by DMFT [39, 40, 42]. Two-dimensional spin-fluctuations and superconductivity, however, cannot be described. For describing such physics, non-local correlations beyond DMFT are needed.

For the nickelates, the oxygen bands are at a much lower energy. Hence, as indicated in the right side panel of **Figure 2**, the lower Ni $3d_{x^2-y^2}$ Hubbard band can be expected to be closer to the Fermi energy than the oxygen p orbitals [32, 33]. Consequently, undoped nickelates would be Mott–Hubbard insulators if it was not for two additional bands that cross E_F around the Γ- and A-momentum. These form electron pockets, as visualized in **Figure 2** (bottom right), and self-dope the Ni $3d_{x^2-y^2}$ band away from half-filling. As the $3d_{x^2-y^2}$ is doped, it develops, even when the Coulomb interaction is large, a quasiparticle peak at the Fermi energy as displayed in the right side panel of **Figure 2**.

3 IRRELEVANCE OF VARIOUS ORBITALS

Next, we turn to various orbitals that may appear relevant at first glance but turn out to be irrelevant for the low-energy physics

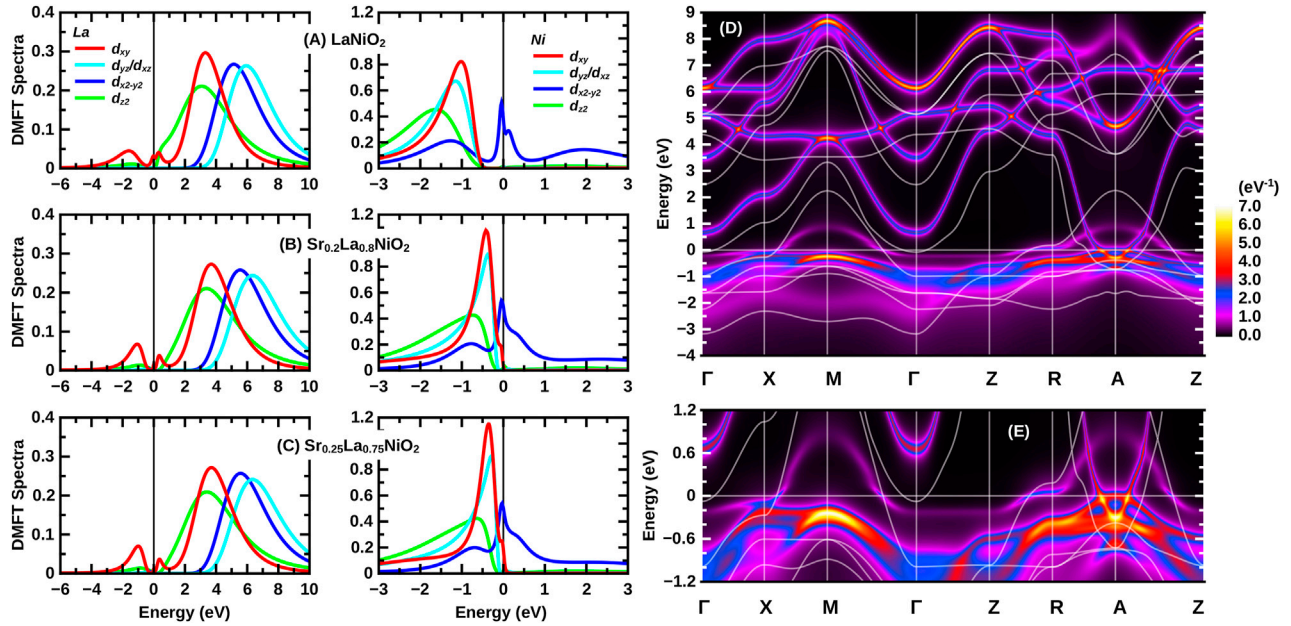

FIGURE 3 | DMFT *k*-integrated **(A–C)** and *k*-resolved **(D,E)** spectral functions $A(\omega)$ and $A(k, \omega)$ of undoped $LaNiO_2$ **(A)**, 20% Sr-doped $LaNiO_2$ ($Sr_{0.2}La_{0.8}NiO_2$) **(B)**, and 25% Sr-doped $LaNiO_2$ ($Sr_{0.25}La_{0.75}NiO_2$) **(C)**. The *k*-resolved spectral function $A(k, \omega)$ of $La_{0.8}Sr_{0.2}NiO_2$ is shown in **(D)**; **(E)** is a zoom-in of **(D)**. Data partially obtained from [33, 55].

when taking electronic correlations properly into account. To account for the latter, we use DFT + DMFT [50–54], which is the state of the art for calculating correlated materials.

Oxygen Orbitals

For nickelates, the oxygen 2*p* orbitals are approximately 3 eV lower in energy than in cuprates within DFT. Hence, some DFT + DMFT calculations did not include these from the beginning [32, 33], and those that did [22] also found the oxygen 2*p* orbitals at a lower energy than the lower Ni $3d_{x^2-y^2}$ Hubbard band. Hence, while there is still some hybridization and mixing between the O 2*p* states and the Ni $3d_{x^2-y^2}$ states, a projection onto a low-energy set of orbitals without oxygen appears possible.

Ni $3d_{3z^2-r^2}$ and t_{2g} Orbitals

Instead of the oxygen 2*p* orbitals, the DFT calculation in **Figure 2** and elsewhere [10, 11, 17, 48] show other Ni 3*d* orbitals closely below the Ni $3d_{x^2-y^2}$ band. In fact, these other 3*d* orbitals are somewhat closer to the Fermi level than in the case of cuprates. Electronic correlations can strongly modify the DFT band structure. In particular, the Hund's exchange J tends to drive the system toward a more equal occupation of different orbitals, especially if there is more than one hole (more than one unpaired electron) in the Ni 3*d* orbitals. This is not only because a larger local spin is made possible but also because the inter-orbital Coulomb interaction U' between two electrons in two different orbitals is smaller than the intra-orbital Coulomb interaction $U = U' + 2J$ for two electrons in the same orbital. This tendency is countered by the crystal field splitting (local DFT potentials) which puts the $3d_{x^2-y^2}$ orbital above the Ni $3d_{3z^2-r^2}$ orbital and the other (t_{2g}) Ni 3*d* orbitals because of the absence of apical O atoms in NiO_4 squares.

Figure 3 shows the DFT + DMFT spectral function for $Sr_xLa_{1-x}NiO_2$ from 0 to 25% Sr-doping. In these calculations [33], all Ni 3*d* and all La 5*d* orbitals have been taken into account in a WIEN2WANNIER [56] projection supplemented by interactions calculated within the constrained random phase approximation (cRPA) [55] to be $U' = 3.10$ eV (2.00 eV) and Hund's exchange $J = 0.65$ eV (0.25 eV) for Ni (La). On a technical note, the DMFT self-consistency equations [39] have been solved here at room temperature (300 K) by continuous-time quantum Monte Carlo simulations in the hybridization expansions [57] using the W2DYNAMICS implementation [58, 59] and the maximum entropy code of ANA_CONT [60] for analytic continuation.

Clearly, **Figure 3** indicates that for up to 20% Sr-doping, the other Ni 3*d* orbitals besides the $3d_{x^2-y^2}$ orbital are not relevant for the low-energy physics of $Sr_xLa_{1-x}NiO_2$; they are fully occupied below the Fermi energy. With doping, these other Ni 3*d* orbitals, however, shift more and more upward in energy. At around 25% Sr-doping, they touch the Fermi energy and hence a multi-orbital Ni description becomes necessary at larger dopings. That is, between 20 and 30% Sr-doping, the physics of $Sr_xLa_{1-x}NiO_2$ turns from single to multi-orbital. In the case of $Sr_xNd_{1-x}NiO_2$, this turning point is at slightly larger doping [33]. Later, in **Section 6**, we will see that for the Ni $3d^8$ configuration, which in **Section 6** is induced by topotactic hydrogen and here would be obtained for 100% Sr doping; the two holes in the Ni 3*d* orbitals form a spin-1 and occupy two orbitals: $3d_{x^2-y^2}$ and $3d_{3z^2-r^2}$. In **Figure 3**,we see at 30% doping, the first steps into this direction. Importantly, within the superconducting doping regime which,

noteworthy, is below 24% Sr-doping for $Sr_xNd_{1-x}NiO_2$ [34, 35] and 21% for $Sr_xLa_{1-x}NiO_2$ [61], a single $3d_{x^2-y^2}$ Ni-orbital is sufficient for the low-energy modeling. A one-band Hubbard model description based on DMFT calculations was also concluded in [32] for the undoped parent compound.

DFT + DMFT calculations by Lechermann [22, 23] stress, on the other hand, the relevance of the $3d_{3z^2-r^2}$ orbital. Let us note that also in [22] the number of holes in the $3d_{3z^2-r^2}$ orbital is considerably less than in that in the $3d_{x^2-y^2}$. However, for low Sr-doping, also a small quasiparticle peak develops for the $3d_{3z^2-r^2}$ band [22, 23]. An important difference to [33, 55] is that the $5d$ Coulomb interaction has been taken into account in [33, 55] and that the Coulomb interaction of [22] is substantially larger. The $5d$ Coulomb interaction pushes the Γ pocket above the Fermi energy (see next paragraph). As much of the holes in the $3d_{3z^2-r^2}$ orbital stem from the admixture of this orbital to the Γ pocket, this difference is very crucial for the occupation of the $3d_{3z^2-r^2}$ orbital in some calculations [21, 23]. On the other hand, in GW + extended DMFT calculations by Petocchi *et al.* [24], the $3d_{3z^2-r^2}$ orbital is pushed to the Fermi energy for large k_z instead, that is, around the R, Z, and A point. Except for this large k_z deviation, the Fermi surface, the effective mass of the Ni $3d_{x^2-y^2}$ orbital etc. of [24] are similar to our calculation [33, 62].

First experimental hints on the (ir) relevance of the $3d_{3z^2-r^2}$ can be obtained from resonant inelastic X-ray scattering (RIXS) experiments [63, 64]. Higashi et al. [65] analyzed these RIXS data by comparison with DFT + DMFT and obtained good agreement with the experiment. They conclude that $NdNiO_2$ is slightly doped away from $3d^9$ because of a small self-doping from the Nd $5d$ band and that only the $3d_{x^2-y^2}$ Ni orbital (not the $3d_{3z^2-r^2}$ orbital) is partially filled and that the Ni–O hybridization plays a less important role than for the cuprates.

Γ Pocket

A feature clearly present in DFT calculations for the nickelate parent compounds $LaNiO_2$ and $NdNiO_2$ is the Γ pocket, see **Figure 2D**. However, when the Coulomb interaction on the La or Nd sites is included, it is shifted upward in energy. Furthermore, Sr-doping depopulates the Ni $3d_{x^2-y^2}$ orbital and the A and Γ pocket, and, thus, also helps pushing the Γ pocket above the Fermi energy. Clearly in the DFT + DMFT k-resolved spectrum of **Figure 3**, the Γ pocket is above the Fermi energy. To some extent, the presence or absence of the Γ pocket also depends on the rare-earth cation. For $NdNiO_2$, we obtain a Γ pocket for the undoped compound [33], which only shifts above the Fermi energy with Sr-doping in the superconducting region, whereas for $LaNiO_2$, it is already above the Fermi level without Sr-doping. We can hence conclude that while there might be a Γ pocket without Sr-doping, DFT + DMFT results suggest that it is absent in the superconducting doping regime.

Briefly after the discovery of superconductivity in nickelates, it has also been suggested that the Nd $5d$ orbitals of the pockets couple to the Ni $3d_{x^2-y^2}$ spin giving rise to a Kondo effect [20, 66]. However, **Table 1** shows that the hybridization between the relevant Ni $3d_{x^2-y^2}$ and the most important La or Nd $5d_{xy}$ and $5d_{3z^2-r^2}$ vanishes by symmetry. Also, the full 5 Ni and 5 Nd band DMFT calculations in **Figure 3** do not show a hybridization (gap) between A pocket and Ni bands. This suggests that the Γ and A pocket are decoupled from the $3d_{x^2-y^2}$ orbitals. There is no hybridization and hence no Kondo effect.

Nd 4*f* Orbitals

Finally, the importance of the Nd $4f$ orbitals has been suggested in the literature. Treating these $4f$ orbitals in DFT is not trivial because DFT puts them in the vicinity of the Fermi level. This neglects that electronic correlations split the Nd $4f$ into upper and lower Hubbard bands as they form a local spin. This effect is beyond DFT. One way to circumvent this difficulty is to put the Nd $4f$ orbitals in the core instead of having them as valence states close to the Fermi energy. This is denoted as "GGA open core" instead of standard "GGA" in **Table 1**. The localized Nd $4f$ spins might, in principle, be screened through a Kondo effect. However, the hybridization of the Nd $4f$ with the Ni $3d_{x^2-y^2}$ orbital at the Fermi energy is extremely small, see **Table 2** and [67]. Hence, the Kondo temperature is zero for all practical purposes. In spin-polarized DFT + U, there is, instead, a local exchange interaction between the Nd $4f$ and the predominately Nd $5d$ Γ pocket [68]. However, as pointed out in the previous paragraph, the Γ pocket is shifted above the Fermi level in the superconducting Sr-doping regime. Hence in [33], we ruled out that the Nd $4f$ is relevant for superconductivity. This has been spectacularly confirmed experimentally by the discovery of superconductivity in nickelates without f electrons: $Ca_xLa_{1-x}NiO_2$ [69] and $Sr_xLa_{1-x}NiO_2$ [61] have a similar T_c.

4 ONE-BAND HUBBARD MODEL PLUS RESERVOIR

Altogether, this leaves us with **Figures 1B,D** as the arguably simplest model for nickelate superconductors, consisting of a strongly correlated Ni $3d_{x^2-y^2}$ band and an A pocket. This A pocket is derived from the Nd $5d_{xy}$ band which, however, crosses the Ni $3d$ orbitals and hybridizes strongly with the Ni t_{2g} orbitals so that at the bottom of the A pocket, that is, at the momentum A, it is made up primarily from Ni t_{2g}, whereas the Nd $5d_{xy}$ contribution is here at a lower energy. This makes the A pocket much more resistive to shifting up in energy than the Γ pocket.

On the other hand, the A pocket does not interact with the Ni $3d_{x^2-y^2}$ band; that is, does not hybridize in **Table 1**. Hence, we can consider the A pocket as a mere hole reservoir which accommodates part of the holes induced by Sr-doping, whereas the other part goes into the correlated Ni $3d_{x^2-y^2}$ band which is responsible for superconductivity. **Figure 4** shows the thus obtained Ni $3d_{x^2-y^2}$ occupation as a function of Sr-doping in the DFT + DMFT calculation with 5 Ni and 5 Nd(La) orbitals.

It is noted that $NdNiO_2$ shows for Sr-doping below about 10% more holes in the Ni $3d_{x^2-y^2}$ orbital and a weaker dependence on the Sr-doping since here the Γ pocket is still active, not only taking away electrons from Ni but also first absorbing some of the holes from the Sr-doping until it is completely depopulated (shifted above the Fermi energy) before superconductivity sets in.

TABLE 1 | Hybridization (hopping amplitude in eV) between the partially occupied Ni $3d_{x^2-y^2}$ and the La/Nd 5*d* orbitals [33]. Here, the results are obtained from Wannier projections onto 17-bands (La/Nd-4*f* + La/Nd-5*d* + Ni-3*d*) and 10-bands (La/Nd-5*d* + Ni-3*d*).

$LaNiO_2$	La $5d_{xy}$	La $5d_{yz}$	La $5d_{xz}$	La $5d_{x^2-y^2}$	La $5d_{z^2}$
Ni $3d_{x^2-y^2}$ (10-band model, GGA)	0.000	0.084	−0.084	−0.017	0.000
Ni $3d_{x^2-y^2}$ (17-band model, GGA)	0.000	0.085	−0.085	−0.037	0.000
$NdNiO_2$	**Nd $5d_{xy}$**	**Nd $5d_{yz}$**	**Nd $5d_{xz}$**	**Nd $5d_{x^2-y^2}$**	**Nd $5d_{z^2}$**
Ni $3d_{x^2-y^2}$ (10-band model, GGA open core)	0.000	0.070	−0.070	−0.038	0.000
Ni $3d_{x^2-y^2}$ (10-band model, GGA)	0.000	0.077	−0.077	−0.006	0.000
Ni $d_{x^2-y^2}$ (17-band model, GGA)	0.000	0.081	−0.081	−0.023	0.000

TABLE 2 | Hybridization (hopping amplitude in eV) between the Ni $3d_{x^2-y^2}$ and the Nd (La) 4*f* orbitals, as obtained from Wannier projections onto 17-bands (La/Nd-4*f* + La/Nd-5*d* + Ni-3*d*), including the 4*f* as valence states in DFT (GGA) [33].

$LaNiO_2$ (GGA)	f_{xz^2}	f_{yz^2}	f_{z^3}	$f_{x(x^2-3y^2)}$	$f_{y(3x^2-y^2)}$	$f_{z(x^2-y^2)}$	f_{xyz}
Ni-$d_{x^2-y^2}$	−0.030	0.030	0.000	−0.085	−0.085	−0.020	−0.000
$NdNiO_2$ (GGA)	**f_{xz^2}**	**f_{yz^2}**	**f_{z^3}**	**$f_{x(x^2-3y^2)}$**	**$f_{y(3x^2-y^2)}$**	**$f_{z(x^2-y^2)}$**	**f_{xyz}**
Ni-$d_{x^2-y^2}$	−0.021	0.021	0.000	−0.061	−0.061	0.016	−0.000

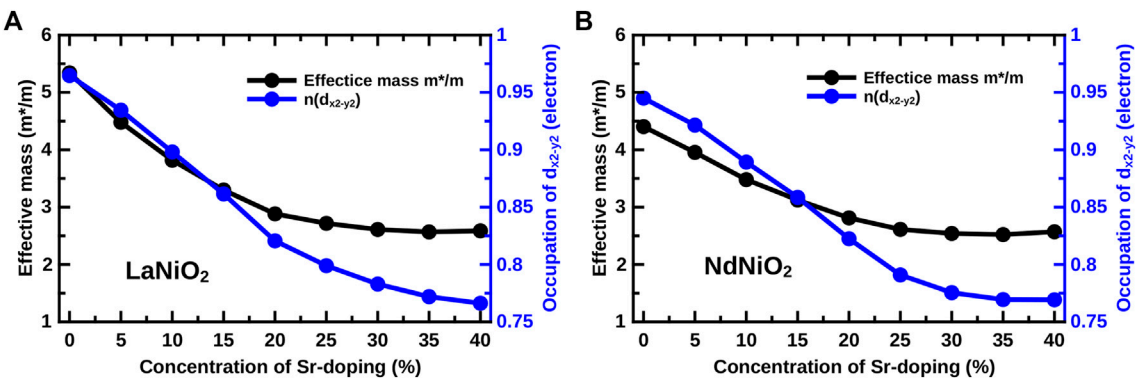

FIGURE 4 | Occupation of the Ni $3d_{x^2-y^2}$ orbital (blue; right *y*-axis) and its effective mass enhancement $m^*/m = 1/Z$ (black; left *y*-axis in panels) vs. Sr-doping for $LaNiO_2$ **(A)** and $NdNiO_2$ **(B)** as calculated in DFT + DMFT. From [33] (Supplemental material).

In the subsequent one-band calculation, presented in the next paragraph, we employ the occupation from the Ni $3d_{x^2-y^2}$ orbital as calculated in this full DMFT calculation with 5 Ni and 5 Nd orbitals. This accounts not only for the electron pocket in the DMFT calculation but also for minor hybridization effects between the Ni $3d_{x^2-y^2}$ and $3d_{3z^2-r^2}$ orbital, for example, along the Γ-*X* direction. In principle, this hybridization effect, which inter-mixes the orbital contribution to the bands, should not be taken into account in the one-band Hubbard model. This aims at modeling the effective $3d_{x^2-y^2}$ band which is crossing the Fermi level and which is predominantly Ni $3d_{x^2-y^2}$ (but also has admixtures from the other orbitals because of the hybridization). In the case of the Ni $3d_{x^2-y^2}$ orbital, this hybridization is very weak [33] (Supplemental Material) and can be neglected as a first approximation [62] (Supplemental Material). For other Ni 3*d* orbitals, this hybridization has a sizeable effect on their respective occupation. For example, the Ni $3d_{3z^2-r^2}$ orbital which is strongly hybridizing with the Nd $5d_{3z^2-r^2}$ orbital only has an occupation of 1.85 electrons per site in our multi-orbital calculation [62] (Supplemental material), whereas the effective Ni $3d_{3z^2-r^2}$ orbital, including contributions from the hybridization, is fully occupied with two electrons per site as it is completely below the Fermi level.

The hopping parameters for the Ni-$3d_{x^2-y^2}$ model from a one-band Wannier projection are shown in **Table 3** and compared to that of the same orbital in a 10-band and 17-band Wannier projection. Here, t_{R_x,R_y,R_z} denotes the hopping by R_i unit cells in the *i* direction. That is, t_{000} is the on-site potential, $t = -t_{100}$; $t' = -t_{110}$, and $t'' = -t_{200}$ are the nearest, next-nearest, and next-next-nearest neighbor hopping, respectively; and $t_z = -t_{001}$ is the hopping in the *z*-direction perpendicular to the NiO_2 planes. The hopping parameters are strikingly similar for $LaNiO_2$ and $NdNiO_2$ and the different Wannier projections.

Besides the doping from **Figure 4** and the hopping for the one-band Wannier projection from **Table 3**, we only need the interaction parameter for doing realistic one-band Hubbard

TABLE 3 | Major hopping elements (in units of eV) of the Ni-$3d_{x^2-y^2}$ orbital from 1-band (Ni-$3d_{x^2-y^2}$), 10-bands (La/Nd-*d* + Ni-*d*), and 17-bands (La/Nd-*f* + La/Nd-*d* + Ni-*d*) Wannier projections. The DFT-relaxed lattice parameters are as follows: $LaNiO_2$ ($a = b = 3.88$ Å, $c = 3.35$ Å), $NdNiO_2$ ($a = b = 3.86$ Å, $c = 3.24$ Å) [33].

$LaNiO_2$ (GGA)	t_{000}	t_{100}	t_{001}	t_{110}	t_{200}	t_{210}
1-band (Ni-$d_{x^2-y^2}$)	0.2689	−0.389	−0.036	0.097	−0.046	−0.003
10-bands (La-*d* + Ni-*d*)	0.295	−0.397	−0.045	0.098	−0.049	0.000
17-bands (La-*f* + La-*d* + Ni-*d*)	0.351	−0.394	−0.023	0.079	−0.042	−0.000
$NdNiO_2$ (GGA open core)	t_{000}	t_{100}	t_{001}	t_{110}	t_{200}	t_{210}
1-band (Ni-$d_{x^2-y^2}$)	0.305	−0.394	−0.033	0.095	−0.047	−0.003
10-bands (Nd-*d* + Ni-*d*)	0.316	−0.397	−0.038	0.094	−0.048	−0.000

model calculations for nickelates. In cRPA for a single $3d_{x^2-y^2}$ orbital, one obtains $U = 2.6$ eV [15, 17] at zero frequency. But, the cRPA interaction has strong frequency dependence because of the screening of all the other Ni and Nd (La) orbitals close by. To mimic this frequency dependence, the static U parameter needs to be slightly increased. Expertise from many DFT + DMFT calculations for transition metal oxides shows that it typically needs to be about 0.5 eV larger, so that $U = 3.2$ eV $= 8t$ is reasonable. Altogether, this defines a one-band Hubbard model for nickelates at various dopings. For the conductivity and other transport properties, the A pocket may be relevant as well, but superconductivity should arise from the correlated $3d_{x^2-y^2}$ band that is hardly coupled to the A pocket.

5 NON-LOCAL CORRELATIONS AND SUPERCONDUCTING PHASE DIAGRAM

DFT provides a first picture of the relevant orbitals, and DMFT adds to this effect of strong local correlations, such as the splitting into Hubbard bands, the formation of a quasiparticle peak, and correlation-induced orbital shifts, such as the upshift of the Γ pocket. However, at low temperatures, non-local correlations give rise to additional effects. Relevant factors are as follows: the emergence of strong spin fluctuations and their impact on the spectral function and superconductivity.

For including such non-local correlations, diagrammatic extensions of DMFT, such as the dynamical vertex approximation (DΓA) [36–38, 70], have been proven extremely powerful. Such calculations are possible down to the temperatures of the superconducting phase transition in the correlated regime and for very large lattices so that the long-range correlations close to a phase transition can be properly described. Even (quantum) critical exponents can be calculated [71–74]. DΓA has proven reliable compared with the numerically exact calculations where these are possible [75] and, in particular, provide for a more accurate determination of T_c [76] since the full local frequency dependence of the two-particle vertex is included. Such local frequency dependence can affect even the non-local pairing through spin fluctuations. In, for example, RPA, this frequency dependence and the suppression of the pairing vertex for small frequencies can only be improperly mimicked by (quite arbitrarily) adjusting the static U.

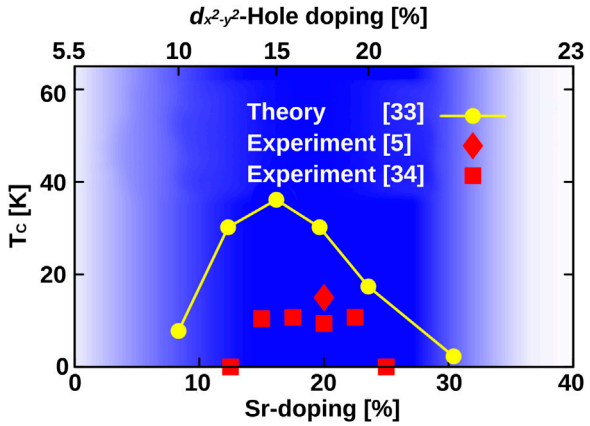

FIGURE 5 | Superconducting phase diagram T_c vs. x for $Sr_xNd_{1-x}NiO_2$ as predicted by DΓA [33] and experimentally confirmed a posteriori in [34, 35]. A priori, that is, at the time of the calculation, only one experimental data point [5] was available. For such a difficult to determine quantity as the superconducting T_c and without adjusting parameters, the accuracy is astonishing. The bottom x-axis shows the Sr-doping and the top x-axis the calculated hole doping of the $3d_{x^2-y^2}$ band according to **Figure 4**. Adjusted from [33].

This simple one-band Hubbard model in DΓA has been the basis for calculating the phase diagram T_c vs. Sr-doping in **Figure 5** [33]. At the time of the calculation, only a single experimental T_c at 20% Sr-doping was available [5]. The physical origin of the superconductivity in these calculations is strong spin fluctuations which form the pairing glue for high-temperature superconductivity. Charge fluctuations are much weaker; the electron–phonon coupling has not been considered and is also too weak for transition metal oxides to yield high-temperature superconductivity. The theoretical T_c in **Figure 5** at 20% doping was from the very beginning slightly larger than in the experiment. Most likely, this is because in the ladder DΓA [36, 37] calculation of T_c, the spin fluctuations are first calculated and then enter the superconducting particle–particle channel [76]. This neglects the feedback effect of these particle–particle fluctuations on the self-energy and the spin fluctuations, which may, in turn, suppress the tendency toward superconductivity somewhat. Such effects would be only included in a more complete parquet DΓA calculation [77–79]. Also, the ignored weak three-dimensional dispersion will

suppress Tc. Let us note that antiferromagnetic spin fluctuations have recently been observed experimentally [64, 80].

Given the slight overestimation of T_c from the very beginning, the agreement with the subsequently obtained experimental T_c vs. Sr-doping x phase diagram [34, 35] in **Figure 5** is astonishingly good. We further see that the superconducting doping regime also concurs with the doping regime where a one-band Hubbard model description is possible for $Sr_xNd_{1-x}NiO_2$, as concluded from a full DFT + DMFT calculation for 5 Ni plus 5 Nd bands. This regime is marked dark blue in **Figure 5** and, as already noted, extends to somewhat larger dopings [33] than for $Sr_xLa_{1-x}NiO_2$ shown in **Figure 3**. Concomitant with this is the fact that the experimental superconducting doping range for $Sr_xLa_{1-x}NiO_2$ extends to a larger x than for $Sr_xNd_{1-x}NiO_2$. For dopings larger than the dark blue regime in **Figure 5**, two Ni $3d$ bands need to be included. As we will show in the next section, this completely changes the physics and is not favorable for superconductivity. For dopings smaller than the dark blue regime in **Figure 5**, on the other hand, the Γ pocket may become relevant for $Sr_xNd_{1-x}NiO_2$, as well as its exchange coupling to the $4f$ moments.

Our theoretical calculations also reveal ways to enhance T_c. Particularly promising is to enhance the hopping parameter t. This enhances T_c because (i) t sets the energy scale of the problem, and a larger t means a larger T_c if U/t, t'/t, and t''/t and doping are kept fixed. Furthermore, the ratio $U/t = 8$ for nickelates is not yet optimal. Indeed, (ii) a somewhat smaller ratio U/t would imply a larger T_c at fixed t [33]. Since the interaction U is local, it typically varies much more slowly when, for example, applying compressive strain or pressure and can be assumed to be constant as a first approximation (for secondary effects, see [81, 82]). Thus, compressive strain or pressure enhance (i) t and reduce (ii) U/t. Both effects enhance T_c. This prediction made in [33] has been confirmed experimentally: applying a pressure of 12 GPa increases T_c from 18K to 31 K in $Sr_{0.18}Pr_{0.82}NiO_2$ [83]. This is so far the record T_c for nickelates, and there are yet no signs for saturation or maximum, indicating that even higher T_c's are possible at higher pressures.

Alternatives to enhance t are 1) to substitute the $SrTiO_3$ substrate by a substrate with smaller in-plane lattice constants since the nickelate film in-plane axis parameters will be locked to that of the substrate. Furthermore, one can 2) replace $3d$ Ni by $4d$ Pd, that is, try to synthesize Nd (La)PdO_2 [11]. Since the Pd $4d$ orbitals are more extended than the $3d$ Ni orbitals, this should enhance t as well.

Next, we turn to the DΓA spectra, more precisely Fermi surfaces, in **Figure 6**. Here, beyond quasiparticle renormalizations of DMFT, non-local spin fluctuations can further impact the spectrum. Only the spectral function of the Hubbard model is shown, describing the $3d_{x^2-y^2}$ band. Please keep in mind that on top of the Fermi surface in **Figure 6**, there is also a weakly correlated A pocket. As one can see in **Figure 6**, antiferromagnetic spin-fluctuations lead to a pseudogap at the antinodal momenta $(\pm\pi, 0)$ $(0, \pm\pi)$ if the filling of the $3d_{x^2-y^2}$ band is close to half-filling. Indeed $n_{3d_{x^2-y^2}} = 0.95$ is the filling for the undoped parent compound $NdNiO_2$ where the A- and Γ

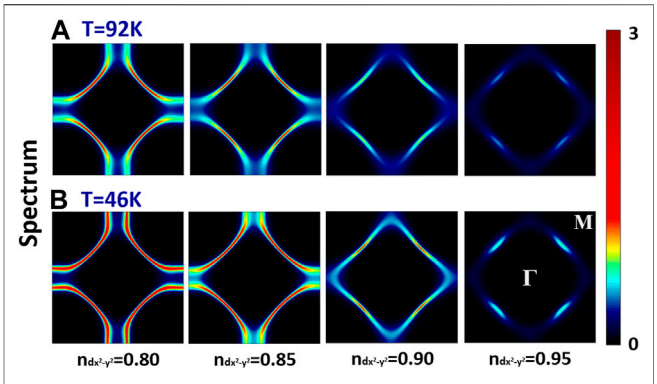

FIGURE 6 | DΓA k-resolved spectrum at the Fermi energy for $T = 0.02t$ = 92 K **(A)** and $T = 0.01t$ = 46 K **(B)** and four different dopings $n_{d_{x^2-y^2}}$ of the Ni-$3d_{x^2-y^2}$ band (left to right). From [33].

pocket have taken 5% of the electrons away from the Ni $3d_{x^2-y^2}$ band. An Sr-doping of 20% is in between $n_{3d_{x^2-y^2}} = 0.85$ and $n_{3d_{x^2-y^2}} = 0.8$, see **Figure 4**. Comparing these theoretical predictions with the experimental Fermi surface, even the **k**-integrated spectrum is very much sought after. However, here, we face the difficulty that the superconducting samples require a $SrTiO_3$ capping layer or otherwise may oxidize out of vacuum. This hinders photoemission spectroscopy (PES) experiments as these are extremely surface-sensitive. Hitherto, PES is only available without the capping layer for $Sr_xPr_{1-x}NiO_2$ [84]. These show a surprisingly low spectral density at the Fermi energy despite the metallic behavior of the doped system, raising the question of how similar these films are to the superconducting films.

6 TOPOTACTIC HYDROGEN: TURNING THE ELECTRONIC STRUCTURE UPSIDE DOWN

The fact that it took 20 years from the theoretical prediction of superconductivity in rare-earth nickelates to the experimental realization already suggests that the synthesis is far from trivial. This is because nickel has to be in the unusually low oxidation state Ni^{+1}. The recipe of success for nickelate superconductors is a two-step process [85]: First, doped perovskite films Sr $(Ca)_xNd$ $(La,Pr)_{1-x}NiO_3$ films are deposited on a $SrTiO_3$ substrate by pulsed laser deposition. Already, this first step is far from trivial, not least because the doped material has to be deposited with homogenous Sr (Ca) concentration. Second, $Sr(Ca)_xNd(La,Pr)_{1-x}NiO_3$ needs to be reduced to $Sr(Ca)_xNd(La,Pr)_{1-x}NiO_2$. To this end, the reducing agent CaH_2 is used. Here, the problem is that this reduction might be incomplete with excess oxygen remaining or that hydrogen from CaH_2 is topotactically intercalated in the Sr $(Ca)_xNd$ $(La,Pr)_{1-x}NiO_2$ structure. A particular difficulty is that the light hydrogen is experimentally hard to detect, for example, it evades conventional X-ray structural detection.

In [55], we studied the possibility to intercalate hydrogen, that is, to synthesize unintendedly $Sr_xNd(La)_{1-x}NiO_2H$ instead of $Sr_xNd(La)_{1-x}NiO_2$. For the reduction of, for example, $SrVO_3$

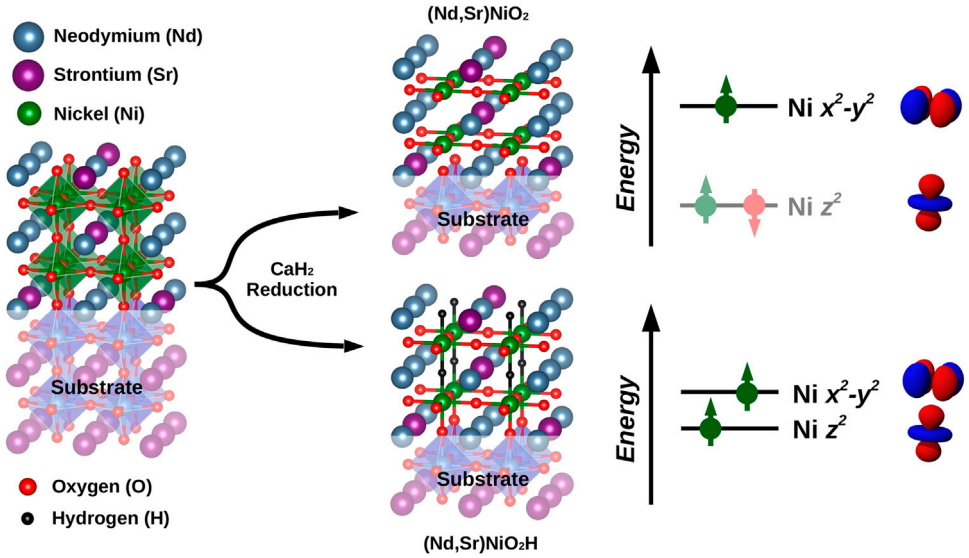

FIGURE 7 | Reduction of $Sr_xNd(La)_{1-x}NiO_3$ with CaH_2 may result not only in the pursued end product $Sr_xNd(La)_{1-x}NiO_2$ but also in $Sr_xNd(La)_{1-x}NiO_2H$, where H atoms occupy the vacant O sites between the layers. This has dramatic consequences for the electronic structure. In a first, purely local picture, visualized on the right side, there is instead of Ni $3d^9$ with one-hole in the $3d_{x^2-y^2}$ orbital, two holes in the $3d_{x^2-y^2}$ and $3d_{3z^2-r^2}$ orbital forming a local spin-1.

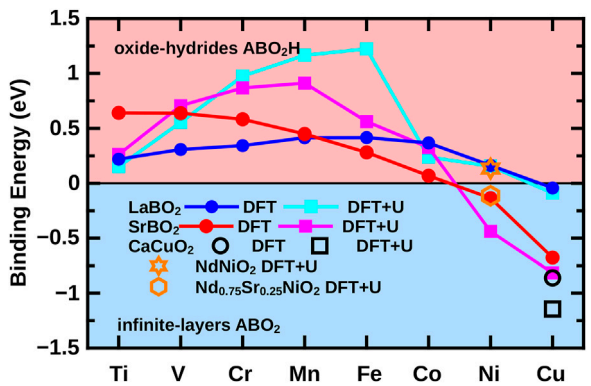

FIGURE 8 | Binding energy for topotactical H as calculated by non–spin-polarized DFT and spin-polarized DFT + U for various transition metals *B* (*x*-axis). Positive binding energies indicate that $ABNiO_2H$ is energetically favored; for negative binding energies, $ABNiO_2$ is more stable. The data for non–spin-polarized DFT calculations are from [55].

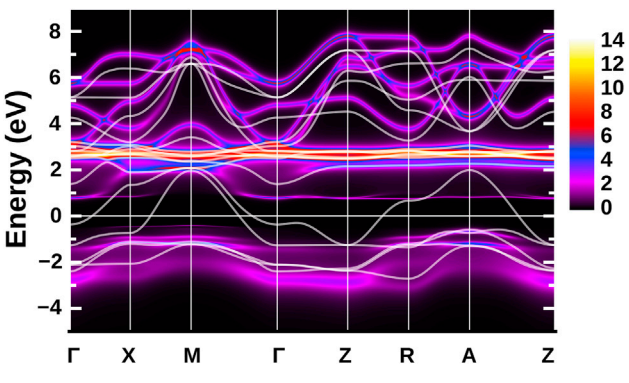

FIGURE 9 | DFT (white lines) and DMFT (color bar) *k*-resolved spectral function for $LaNiO_2H$. Here, a model with La-d + La-f + Ni-d was used, which is beyond the Ni-d only and La-d + Ni-d models shown in [55].

with CaH_2, it is well-established that $SrVO_2H$ may be obtained as the end product [86]. Both possible end products are visualized in **Figure 7**. The extra H takes away one more electron from the Ni sites. Hence, we have two holes on the Ni sites which in a local picture are distributed to two orbitals and form a spin-1, due to Hund's exchange.

The first question is how susceptible the material is to bind topotactic H. To answer this question, one can calculate the binding energy E ($ABNiO_2$) + 1/2 E (H_2)- E ($ABNiO_2H$) in DFT [55, 87]. The result is shown in **Figure 8**, which clearly shows that early transition metal oxides are prone to intercalate hydrogen, whereas for cuprates, the infinite layer compound without H is more stable. Nickelates are in-between. For the undoped compounds $NdNiO_2$, and even a bit more for $LaNiO_2$, it is favorable to intercalate H. However, for the Sr-doped nickelates, the energy balance is inverted. Here, it is unfavorable to bind hydrogen.

Let us emphasize that this is only the enthalpy balance. In the actual synthesis also the reaction kinetics matter, and the entropy which is large for the H_2 gas. Nonetheless, this shows that undoped nickelates are very susceptible to topotactic H. This possibly means that, experimentally, not a complete H-coverage as in $ABNiO_2H$ of **Figure 8** is realized, but some hydrogen may remain in the nickelates because of an incomplete reduction with CaH_2. Indeed, hydrogen remainders have later been detected experimentally by nuclear magnetic resonance (NMR) spectroscopy, and they have even been used to analyze the antiferromagnetic spin fluctuations [80].

Now that we have established that remainders of hydrogen can be expected for nickelates at low doping, the question is how this affects the electronic structure. The local picture of **Figure 7** already suggested a very different electronic configuration. This is further corroborated by DFT + DMFT calculations for $LaNiO_2H$ presented in **Figure 9**. Here, the DFT band structure shows a metallic behavior with two orbitals, Ni $3d_{x^2-y^2}$ and $3d_{3z^2-r^2}$, crossing the Fermi level. There are no rare-earth electron pockets any longer. Thus, we have an undoped Ni $3d^8$ configuration without Sr-doping. If electronic correlations are included in DMFT, the DFT bands split into two sets of Hubbard bands. Above the Fermi level, one can identify the upper $3d_{x^2-y^2}$ and $3d_{3z^2-r^2}$ Hubbard band below the flat *f* bands in **Figure 9**, with some broadening because of the electronic correlations. The lower Hubbard bands intertwine with the Ni t_{2g} orbitals below the Fermi energy.

Even if we dope $LaNiO_2H$, this electronic structure is not particularly promising for superconductivity. First, it is not two-dimensional because of the $3d_{3z^2-r^2}$ orbitals, which makes the system more three-dimensional. More specifically, there is a considerable hopping process from Ni $3d_{3z^2-r^2}$ *via* H to the Ni $3d_{3z^2-r^2}$ on the vertically adjacent layer, as evidenced in **Figure 9** by the DFT dispersion of this band in the Γ-Z direction; the other $3d_{x^2-y^2}$ band is (as expected) flat in this direction. Second, the tendency to form local magnetic moments of spin-1 counteracts the formation of Cooper pairs from two spin-1/2s. Hence, altogether, we expect topotactic H to prevent high-temperature superconductivity.

7 CONCLUSION

In this article, we have discussed the physics of nickelate superconductors from the perspective of a one-band Hubbard model for the Ni $3d_{x^2-y^2}$ band plus an *A* pocket. Because of symmetry, this *A* pocket does not hybridize with the $3d_{x^2-y^2}$ band and merely acts as a decoupled electron reservoir. Hence, once the filling of the $3d_{x^2-y^2}$ band is calculated as a function of Sr- or Ca-doping in $Sr(Ca)_xNd(La,Pr)_{1-x}NiO_2$, we can, for many aspects, concentrate on the physics of the thus doped Hubbard model. This includes antiferromagnetic spin fluctuations and the onset of superconductivity. Other physical properties, such as transport and the Hall conductivity, depend, as a matter of course, also on the *A* pocket. This is in stark contrast to the cuprates, where the oxygen *p* orbitals are much closer to the Fermi level so that we have a charge-transfer insulator that needs to be modeled by the more complex Emery model.

The one-band Hubbard model picture for nickelates was put forward early on for nickelates [11, 19, 32, 33], and its proper doping, including correlation effects, has been calculated in [33]. This picture has been confirmed by many experimental observations so far. The Nd 4*f* states are, from the theoretical perspective, irrelevant because they form a local spin and barely hybridize with the $3d_{x^2-y^2}$ band. This has been confirmed experimentally by the observation of superconductivity in $Sr(Ca)_xLa_{1-x}NiO_2$. The minor importance of the other Ni 3*d* orbitals, in particular the $3d_{3z^2-r^2}$ orbital, is indicated through the careful analysis [65] of RIXS data [63, 64]. Not confirmed experimentally is hitherto the prediction that the Γ pocket is shifted above the Fermi level in the superconducting doping regime.

Strong evidence for the one-band Hubbard model picture is the prediction of the superconducting phase diagram [33], confirmed experimentally in [34, 35]. A further prediction was the increase of T_c with pressure or compressive strain [33], which was subsequently found in the experiment with a record $T_c = 31$ K for nickelates under pressure [83]. The strength of antiferromagnetic spin-fluctuations as obtained in RIXS [64] also roughly agrees with that of the calculation [33]. Altogether, this gives us quite some confidence in the one-band Hubbard model scenario, which even allowed for a rough calculation of T_c. Notwithstanding, further theoretical calculations, in particular including non-local correlations also in a realistic multi-orbital setting [37, 70, 88], are eligible. On the experimental side more detailed, for example, **k**-resolved information is desirable as are further close comparisons between the experiment and theory.

A good analysis of the quality of the samples is also mandatory, especially against the background that superconducting nickelates have been extremely difficult to synthesize. Incomplete oxygen reduction and topotactic hydrogen [55, 87] are theoretically expected to be present because this is energetically favored, at least for low Sr-doping. This leads to two holes in two orbitals forming a high-spin state and a three-dimensional electronic structure, thus obstructing the intrinsic physics of superconducting nickelates.

AUTHOR CONTRIBUTIONS

All authors listed have made a substantial, direct, and intellectual contribution to the study and approved it for publication.

FUNDING

We acknowledge funding through the Austrian Science Funds (FWF), Project numbers P 32044 and P 30213, and Grant-in-Aids for Scientific Research (JSPS KAKENHI), Grant numbers 19H05825, JP20K22342, and JP21K13887. OJ was supported by the Leibniz Association through the Leibniz Competition. Calculations were partially performed on the Vienna Scientific Cluster (VSC).

ACKNOWLEDGMENTS

We thank Atsushi Hariki, Motoaki Hirayama, Josef Kaufmann, Yusuke Nomura, and Terumasa Tadano for valuable discussions.

REFERENCES

1. Anisimov VI, Bukhvalov D, Rice TM. Electronic Structure of Possible Nickelate Analogs to the Cuprates. *Phys Rev B* (1999) 59:7901–6. doi:10.1103/PhysRevB.59.7901
2. Chaloupka J, Khaliullin G. Orbital Order and Possible Superconductivity in $LaNiO_3/LaMO_3$ Superlattices. *Phys Rev Lett* (2008) 100:016404. doi:10.1103/PhysRevLett.100.016404
3. Hansmann P, Toschi A, Yang X, Andersen O, Held K. Electronic Structure of Nickelates: From Two-Dimensional Heterostructures to Three-Dimensional Bulk Materials. *Phys Rev B* (2010) 82:235123. doi:10.1103/PhysRevB.82.235123
4. Hansmann P, Yang X, Toschi A, Khaliullin G, Andersen OK, Held K. Turning a Nickelate Fermi Surface into a Cupratelike One through Heterostructuring. *Phys Rev Lett* (2009) 103:016401. doi:10.1103/PhysRevLett.103.016401
5. Li D, Lee K, Wang BY, Osada M, Crossley S, Lee HR, et al. Superconductivity in an Infinite-Layer Nickelate. *Nature* (2019) 572:624–7. doi:10.1038/s41586-019-1496-5
6. Balestrino G, Medaglia PG, Orgiani P, Tebano A, Aruta C, Lavanga S, et al. Very Large Purely Intralayer Critical Current Density in Ultrathin Cuprate Artificial Structures. *Phys Rev Lett* (2002) 89:156402. doi:10.1103/physrevlett.89.156402
7. Di Castro D, Cantoni C, Ridolfi F, Aruta C, Tebano A, Yang N, et al. High-T_c Superconductivity at the Interface between the $CaCuO_2$ and $SrTiO_3$ Insulating Oxides. *Phys Rev Lett* (2015) 115:147001. doi:10.1103/PhysRevLett.115.147001
8. Orgiani P, Aruta C, Balestrino G, Born D, Maritato L, Medaglia PG, et al. Direct Measurement of Sheet Resistance $R_\square$ in Cuprate Systems: Evidence of a Fermionic Scenario in a Metal-Insulator Transition. *Phys Rev Lett* (2007) 98: 036401. doi:10.1103/PhysRevLett.98.036401
9. Siegrist T, Zahurak S, Murphy D, Roth R. The Parent Structure of the Layered High-Temperature Superconductors. *Nature* (1988) 334:231–2. doi:10.1038/334231a0
10. Botana AS, Norman MR. Similarities and Differences between $LaNiO_2$ and $CaCuO_2$ and Implications for Superconductivity. *Phys Rev X* (2020) 10:011024. doi:10.1103/PhysRevX.10.011024
11. Hirayama M, Tadano T, Nomura Y, Arita R. Materials Design of Dynamically Stable D^9 Layered Nickelates. *Phys Rev B* (2020) 101:075107. doi:10.1103/PhysRevB.101.075107
12. Hu L-H, Wu C. Two-band Model for Magnetism and Superconductivity in Nickelates. *Phys Rev Res* (2019) 1:032046. doi:10.1103/PhysRevResearch.1.032046
13. Jiang M, Berciu M, Sawatzky GA. Critical Nature of the Ni Spin State in Doped $NdNiO_2$. *Phys Rev Lett* (2020) 124:207004. doi:10.1103/PhysRevLett.124.207004
14. Lee K-W, Pickett W. Infinite-layer $LaNiO_2$: Ni^{1+} Is Not Cu^{2+}. *Phys Rev B* (2004) 70:165109. doi:10.1103/PhysRevB.70.165109
15. Nomura Y, Hirayama M, Tadano T, Yoshimoto Y, Nakamura K, Arita R. Formation of a Two-Dimensional Single-Component Correlated Electron System and Band Engineering in the Nickelate Superconductor $NdNiO_2$. *Phys Rev B* (2019) 100:205138. doi:10.1103/PhysRevB.100.205138
16. Pavarini E, Dasgupta I, Saha-Dasgupta T, Jepsen O, Andersen OK. Band-structure Trend in Hole-Doped Cuprates and Correlation with T (C max). *Phys Rev Lett* (2001) 87:047003. doi:10.1103/PhysRevLett.87.047003
17. Sakakibara H, Usui H, Suzuki K, Kotani T, Aoki H, Kuroki K. Model Construction and a Possibility of Cupratelike Pairing in a New D^9 Nickelate Superconductor (Nd, Sr)NiO_2. *Phys Rev Lett* (2020) 125:077003. doi:10.1103/PhysRevLett.125.077003
18. Werner P, Hoshino S. Nickelate Superconductors: Multiorbital Nature and Spin Freezing. *Phys Rev B* (2020) 101:041104. doi:10.1103/PhysRevB.101.041104
19. Wu X, Di Sante D, Schwemmer T, Hanke W, Hwang HY, Raghu S, et al. Robust $D_{x^2-y^2}$ -wave Superconductivity of Infinite-Layer Nickelates. *Phys Rev B* (2020) 101:060504. doi:10.1103/PhysRevB.101.060504
20. Zhang G-M, Yang Y-F, Zhang F-C. Self-Doped Mott Insulator for Parent Compounds of Nickelate Superconductors. *Phys Rev B* (2020) 101:020501. doi:10.1103/PhysRevB.101.020501
21. Adhikary P, Bandyopadhyay S, Das T, Dasgupta I, Saha-Dasgupta T. Orbital-selective Superconductivity in a Two-Band Model of Infinite-Layer Nickelates. *Phys Rev B* (2020) 102:100501. doi:10.1103/PhysRevB.102.100501
22. Lechermann F. Late Transition Metal Oxides with Infinite-Layer Structure: Nickelates versus Cuprates. *Phys Rev B* (2020) 101:081110. doi:10.1103/PhysRevB.101.081110
23. Lechermann F. Multiorbital Processes Rule the $Nd_{1-x}Sr_xNiO_2$ normal State. *Phys Rev X* (2020) 10:041002. doi:10.1103/PhysRevX.10.041002
24. Petocchi F, Christiansson V, Nilsson F, Aryasetiawan F, Werner P. Normal State of $Nd_{1-x}Sr_xNiO_2$ from Self-Consistent *GW* + EDMFT. *Phys Rev X* (2020) 10:041047. doi:10.1103/PhysRevX.10.041047
25. Bandyopadhyay S, Adhikary P, Das T, Dasgupta I, Saha-Dasgupta T. Superconductivity in Infinite-Layer Nickelates: Role of *F* Orbitals. *Phys Rev B* (2020) 102:220502. doi:10.1103/PhysRevB.102.220502
26. Zaanen J, Sawatzky GA, Allen JW. Band Gaps and Electronic Structure of Transition-Metal Compounds. *Phys Rev Lett* (1985) 55:418–21. doi:10.1103/PhysRevLett.55.418
27. Emery VJ. Theory of High–T_c Superconductivity in Oxides. *Phys Rev Lett* (1987) 58:2794–7. doi:10.1103/PhysRevLett.58.2794
28. Gutzwiller MC. Effect of Correlation on the Ferromagnetism of Transition Metals. *Phys Rev Lett* (1963) 10:159–62. doi:10.1103/PhysRevLett.10.159
29. Hubbard J. Electron Correlations in Narrow Energy Bands. *Proc R Soc Lond Ser A, Math Phys Sci* (1963) 276:238–57. doi:10.1098/rspa.1963.0204
30. Kanamori J. Electron Correlation and Ferromagnetism of Transition Metals. *Prog Theor Phys* (1963) 30:275–89. doi:10.1143/ptp.30.275
31. Zhang FC, Rice TM. Effective Hamiltonian for the Superconducting Cu Oxides. *Phys Rev B* (1988) 37:3759–61. doi:10.1103/PhysRevB.37.3759
32. Karp J, Botana AS, Norman MR, Park H, Zingl M, Millis A. Many-Body Electronic Structure of $NdNiO_2$ and $CaCuO_2$. *Phys Rev X* (2020) 10:021061. doi:10.1103/PhysRevX.10.021061
33. Kitatani M, Si L, Janson O, Arita R, Zhong Z, Held K. Nickelate Superconductors – a Renaissance of the One-Band Hubbard Model. *npj Quan Mater* (2020) 5:59, 2020 . arXiv:2002.12230. doi:10.1038/s41535-020-00260-y
34. Li D, Wang BY, Lee K, Harvey SP, Osada M, Goodge BH, et al. Superconducting Dome in $Nd_{1-x}Sr_xNiO_2$ Infinite Layer Films. *Phys Rev Lett* (2020) 125:027001. arxiv:2003.08506. doi:10.1103/PhysRevLett.125.027001
35. Zeng S, Tang CS, Yin X, Li C, Li M, Huang Z, et al. Phase Diagram and Superconducting Dome of Infinite-Layer $Nd_{1-x}Sr_xNiO_2$ Thin Films, arxiv: 2004.11281. *Phys Rev Lett* (2020) 125:147003. doi:10.1103/physrevlett.125.147003
36. Katanin AA, Toschi A, Held K. Comparing Pertinent Effects of Antiferromagnetic Fluctuations in the Two- and Three-Dimensional Hubbard Model. *Phys Rev B* (2009) 80:075104. doi:10.1103/PhysRevB.80.075104
37. Rohringer G, Hafermann H, Toschi A, Katanin AA, Antipov AE, Katsnelson MI, et al. Diagrammatic Routes to Nonlocal Correlations beyond Dynamical Mean Field Theory. *Rev Mod Phys* (2018) 90:025003. doi:10.1103/revmodphys.90.025003
38. Toschi A, Katanin AA, Held K. Dynamical Vertex Approximation; a Step Beyond Dynamical Mean-Field Theory. *Phys Rev B* (2007) 75:045118. doi:10.1103/PhysRevB.75.045118
39. Georges A, Kotliar G, Krauth W, Rozenberg MJ. Dynamical Mean-Field Theory of Strongly Correlated Fermion Systems and the Limit of Infinite Dimensions. *Rev Mod Phys* (1996) 68:13. doi:10.1103/RevModPhys.68.13
40. Georges A, Krauth W. Numerical Solution of the $D = \infty$ Hubbard Model: Evidence for a Mott Transition. *Phys Rev Lett* (1992) 69:1240–3. doi:10.1103/PhysRevLett.69.1240
41. Jarrell M. Hubbard Model in Infinite Dimensions: A Quantum Monte Carlo Study. *Phys Rev Lett* (1992) 69:168–71. doi:10.1103/PhysRevLett.69.168
42. Metzner W, Vollhardt D. Correlated Lattice Fermions in $D = \infty$ Dimensions. *Phys Rev Lett* (1989) 62:324–7. doi:10.1103/PhysRevLett.62.324
43. Blaha P, Schwarz K, Madsen G, Kvasnicka D, Luitz J. *wien2k: An Augmented Plane Wave+ Local Orbitals Program for Calculating crystal Properties* (2001). Wien: TU Wien.
44. Schwarz K, Blaha P, Madsen GKH (2002). Electronic Structure Calculations of Solids Using the Wien2k Package for Material Sciences. *Comp Phys Comm* 147: 71–6. doi:10.1016/S0010-4655(02)00206-0
45. Kresse G, Hafner J. Ab Initio molecular Dynamics for Open-Shell Transition Metals. *Phys Rev B* (1993) 48:13115–8. doi:10.1103/PhysRevB.48.13115

46. Koepernik K, Eschrig H. Full-potential Nonorthogonal Local-Orbital Minimum-Basis Band-Structure Scheme. *Phys Rev B* (1999) 59:1743–57. doi:10.1103/PhysRevB.59.1743
47. Perdew JP, Burke K, Ernzerhof M. Generalized Gradient Approximation Made Simple. *Phys Rev Lett* (1996) 77:3865–8. doi:10.1103/PhysRevLett.77.3865
48. Nomura Y, Arita R. Superconductivity in Infinite-Layer Nickelates (2021). arXiv:2107.12923.
49. Hansmann P, Parragh N, Toschi A, Sangiovanni G, Held K. Importance of *D–P* Coulomb Interaction for High T_c Cuprates and Other Oxides. *New J Phys* (2014) 16:033009. doi:10.1088/1367-2630/16/3/033009
50. Anisimov VI, Poteryaev AI, Korotin MA, Anokhin AO, Kotliar G. First-principles Calculations of the Electronic Structure and Spectra of Strongly Correlated Systems: Dynamical Mean-Field Theory. *J Phys Condens Matter* (1997) 9:7359–67. doi:10.1088/0953-8984/9/35/010
51. Held K. Electronic Structure Calculations Using Dynamical Mean Field Theory. *Adv Phys* (2007) 56:829–926. doi:10.1080/00018730701619647
52. Held K, Nekrasov IA, Keller G, Eyert V, Blümer N, McMahan AK, et al. Realistic Investigations of Correlated Electron Systems with LDA+DMFT. *physica status solidi (b)* (2006) 243:2599–631. Previously appeared as Psi-k Newsletter No. 56 (April 2003). doi:10.1002/pssb.200642053
53. Kotliar G, Savrasov SY, Haule K, Oudovenko VS, Parcollet O, Marianetti CA. Electronic Structure Calculations with Dynamical Mean-Field Theory. *Rev Mod Phys* (2006) 78:865. doi:10.1103/RevModPhys.78.865
54. Lichtenstein AI, Katsnelson MI. Ab Initio calculations of Quasiparticle Band Structure in Correlated Systems: LDA++ Approach. *Phys Rev B* (1998) 57:6884–95. doi:10.1103/PhysRevB.57.6884
55. Si L, Xiao W, Kaufmann J, Tomczak JM, Lu Y, Zhong Z, et al. Topotactic Hydrogen in Nickelate Superconductors and Akin Infinite-Layer Oxides ABO_2. *Phys Rev Lett* (2020) 124:166402. doi:10.1103/PhysRevLett.124.166402
56. Kuneš J, Arita R, Wissgott P, Toschi A, Ikeda H, Held K. Wien2wannier: From Linearized Augmented Plane Waves to Maximally Localized Wannier Functions. *Comput Phys Commun* (2010) 181:1888–95. doi:10.1016/j.cpc.2010.08.005
57. Gull E, Millis AJ, Lichtenstein AI, Rubtsov AN, Troyer M, Werner P. Continuous-time Monte Carlo Methods for Quantum Impurity Models. *Rev Mod Phys* (2011) 83:349–404. doi:10.1103/RevModPhys.83.349
58. Parragh N, Toschi A, Held K, Sangiovanni G. Conserved Quantities of *SU*(2)-Invariant Interactions for Correlated Fermions and the Advantages for Quantum Monte Carlo Simulations. *Phys Rev B* (2012) 86:155158. doi:10.1103/PhysRevB.86.155158
59. Wallerberger M, Hausoel A, Gunacker P, Kowalski A, Parragh N, Goth F, et al. w2dynamics: Local One- and Two-Particle Quantities from Dynamical Mean Field Theory. *Comp Phys Comm* (2019) 235:388–99. doi:10.1016/j.cpc.2018.09.007
60. Kaufmann J, Held K. ana_cont: Python Package for Analytic Continuation (2021). arXiv:2105.11211.
61. Osada M, Wang BY, Goodge BH, Harvey SP, Lee K, Li D, et al. Nickelate Superconductivity without Rare-Earth Magnetism: $(La,Sr)NiO_2$. *Adv Mater* (2021) 33:2104083. doi:10.1002/adma.202104083
62. Worm P, Si L, Kitatani M, Arita R, Tomczak JM, Held K. Correlations Turn Electronic Structure of Finite-Layer Nickelates Upside Down (2021). arXiv:2111.12697.
63. Hepting M, Li D, Jia CJ, Lu H, Paris E, Tseng Y, et al. Electronic Structure of the Parent Compound of Superconducting Infinite-Layer Nickelates. *Nat Mater* (2020) 19:381. doi:10.1038/s41563-019-0585-z
64. Lu H, Rossi M, Nag A, Osada M, Li DF, Lee K, et al. Magnetic Excitations in Infinite-Layer Nickelates. *Science* (2021) 373:213–6. doi:10.1126/science.abd7726
65. Higashi K, Winder M, Kuneš J, Hariki A. Core-level X-ray Spectroscopy of Infinite-Layer Nickelate: LDA + DMFT Study. *Phys Rev X* (2021) 11:041009. doi:10.1103/PhysRevX.11.041009
66. Gu Y, Zhu S, Wang X, Hu J, Chen H. A Substantial Hybridization between Correlated Ni-*D* Orbital and Itinerant Electrons in Infinite-Layer Nickelates. *Commun Phy* (2020) 3:84. doi:10.1038/s42005-020-0347-x
67. Jiang P, Si L, Liao Z, Zhong Z. Electronic Structure of Rare-Earth Infinite-Layer $RNiO_2$ (R = La, Nd). *Phys Rev B* (2019) 100:201106. doi:10.1103/PhysRevB.100.201106
68. Choi M-Y, Lee K-W, Pickett WE. Role of 4*f* States in Infinite-Layer $NdNiO_2$. *Phys Rev B* (2020) 101:020503. doi:10.1103/PhysRevB.101.020503
69. Zeng SW, Li CJ, Chow LE, Cao Y, Zhang ZT, Tang CS, et al. Superconductivity in Infinite-Layer Lanthanide Nickelates (2021). arXiv:2105.13492.
70. Galler A, Thunström P, Gunacker P, Tomczak JM, Held K. Ab Initio dynamical Vertex Approximation. *Phys Rev B* (2017) 95:115107. doi:10.1103/PhysRevB.95.115107
71. Antipov AE, Gull E, Kirchner S. Critical Exponents of Strongly Correlated Fermion Systems from Diagrammatic Multiscale Methods. *Phys Rev Lett* (2014) 112:226401. doi:10.1103/PhysRevLett.112.226401
72. Rohringer G, Toschi A, Katanin A, Held K. Critical Properties of the Half-Filled Hubbard Model in Three Dimensions. *Phys Rev Lett* (2011) 107:256402. doi:10.1103/PhysRevLett.107.256402
73. Schäfer T, Katanin AA, Held K, Toschi A. Interplay of Correlations and Kohn Anomalies in Three Dimensions: Quantum Criticality with a Twist. *Phys Rev Lett* (2017) 119:046402. doi:10.1103/PhysRevLett.119.046402
74. Schäfer T, Katanin AA, Kitatani M, Toschi A, Held K. Quantum Criticality in the Two-Dimensional Periodic anderson Model. *Phys Rev Lett* (2019) 122:227201. doi:10.1103/PhysRevLett.122.227201
75. Schäfer T, Wentzell N, Šimkovic F, He Y-Y, Hille C, Klett M, et al. Tracking the Footprints of Spin Fluctuations: A Multimethod, Multimessenger Study of the Two-Dimensional Hubbard Model. *Phys Rev X* (2021) 11:011058. doi:10.1103/PhysRevX.11.011058
76. Kitatani M, Schäfer T, Aoki H, Held K. Why the Critical Temperature of High-T_c Cuprate Superconductors Is So Low: The Importance of the Dynamical Vertex Structure. *Phys Rev B* (2019) 99:041115. doi:10.1103/PhysRevB.99.041115
77. Li G, Kauch A, Pudleiner P, Held K. The Victory Project v1.0: An Efficient Parquet Equations Solver. *Comp Phys Comm* (2019) 241:146–54. doi:10.1016/j.cpc.2019.03.008
78. Li G, Wentzell N, Pudleiner P, Thunström P, Held K. Efficient Implementation of the Parquet Equations: Role of the Reducible Vertex Function and its Kernel Approximation. *Phys Rev B* (2016) 93:165103. doi:10.1103/physrevb.93.165103
79. Valli A, Schäfer T, Thunström P, Rohringer G, Andergassen S, Sangiovanni G, et al. Dynamical Vertex Approximation in its Parquet Implementation: Application to Hubbard Nanorings. *Phys Rev B* (2015) 91:115115. doi:10.1103/PhysRevB.91.115115
80. Cui Y, Li C, Li Q, Zhu X, Hu Z, feng Yang Y, et al. NMR Evidence of Antiferromagnetic Spin Fluctuations in $Nd_{0.85}Sr_{0.15}NiO_2$. *Chin Phys Lett* (2021) 38:067401. doi:10.1088/0256-307x/38/6/067401
81. Ivashko O, Horio W, Wan M, Christensen N, McNally D, Paris E, et al. Strain-engineering Mott-insulating La_2CuO_4. *Nat Comm* (2019) 10:786. doi:10.1038/s41467-019-08664-6
82. Tomczak JM, Miyake T, Sakuma R, Aryasetiawan F. Effective Coulomb Interactions in Solids under Pressure. *Phys Rev B* (2009) 79:235133. doi:10.1103/PhysRevB.79.235133
83. Wang NN, Yang MW, Chen KY, Yang Z, Zhang H, Zhu ZH, et al. Pressure-induced Monotonic Enhancement of T_c to over 30 K in the Superconducting $Pr_{0.82}Sr_{0.18}NiO_2$ Thin Films (2021). arXiv:2109.12811.
84. Chen Z, Osada M, Li D, Been EM, Chen S-D, Hashimoto M, et al. Electronic Structure of Superconducting Nickelates Probed by Resonant Photoemission Spectroscopy (2021). arXiv:2106.03963.
85. Lee K, Goodge BH, Li D, Osada M, Wang BY, Cui Y, et al. Aspects of the Synthesis of Thin Film Superconducting Infinite-Layer Nickelates. *APL Mater* (2020) 8:041107. doi:10.1063/5.0005103
86. Katayama T, Chikamatsu A, Yamada K, Shigematsu K, Onozuka T, Minohara M, et al. Epitaxial Growth and Electronic Structure of Oxyhydride $SrVO_2H$ Thin Films. *J Appl Phys* (2016) 120:085305. doi:10.1063/1.4961446
87. Malyi OI, Varignon J, Zunger A. Bulk $NdNiO_2$ Is Thermodynamically Unstable with Respect to Decomposition while Hydrogenation Reduces the Instability and Transforms it from Metal to Insulator (2021). arXiv:2107.01790.

88. Tomczak JM, Liu P, Toschi A, Kresse G, Held K. Merging *GW* with DMFT and Non-local Correlations beyond. *Eur Phys J Spec Top* (2017) 226:2565–90. doi:10.1140/epjst/e2017-70053-1

Conflict of Interest: The authors declare that the research was conducted in the absence of any commercial or financial relationships that could be construed as a potential conflict of interest.

Publisher's Note: All claims expressed in this article are solely those of the authors and do not necessarily represent those of their affiliated organizations, or those of the publisher, the editors, and the reviewers. Any product that may be evaluated in this article, or claim that may be made by its manufacturer, is not guaranteed or endorsed by the publisher.